

Gate Voltage Controllable Non-Equilibrium and Non-Ohmic Behavior in Suspended Carbon Nanotubes

Adam W. Bushmaker,[†] Vikram V. Deshpande,[‡] Scott Hsieh,[‡] Marc W. Bockrath,[‡]
and Stephen B. Cronin^{*†}

*Department of Electrical Engineering, University of Southern California, Los Angeles,
California 90089, and Department of Applied Physics, California Institute of
Technology, Pasadena, California 91125*

Received April 1, 2009; Revised Manuscript Received May 28, 2009

ABSTRACT

In this work, we measure the electrical conductance and temperature of individual, suspended quasi-metallic single-walled carbon nanotubes under high voltage biases using Raman spectroscopy, while varying the doping conditions with an applied gate voltage. By applying a gate voltage, the high-bias conductance can be switched dramatically between linear (Ohmic) behavior and nonlinear behavior exhibiting negative differential conductance (NDC). Phonon populations are observed to be in thermal equilibrium under Ohmic conditions but switch to nonequilibrium under NDC conditions. A typical Landauer transport model assuming zero bandgap is found to be inadequate to describe the experimental data. A more detailed model is presented, which incorporates the doping dependence in order to fit this data.

The exceptionally strong electron–phonon coupling in quasi-metallic (qm) single-walled carbon nanotubes (SWNTs) leads to exciting low dimensional physics including Kohn anomalies,^{1–5} charge-density waves,⁶ and Peierls distortions.⁷ Long mean free paths and high electron velocities make nanotubes an ideal system for studying these interesting effects through high-field, quasi-ballistic electron transport.⁸ Thermal heating of suspended SWNTs with power densities several hundred times larger than the surface of the sun (~ 1 MW/cm²) gives rise to nonequilibrium phonon populations^{9–14} and negative differential conductance (NDC). These characteristics are of interest for high frequency applications, such as mixers, that can operate in the gigahertz and terahertz frequency ranges.^{15,16} Furthermore, SWNTs are of great interest for use as high conductance interconnects in advanced integrated circuits. Initial studies of these phenomena have already been carried out; however, a next generation of more sophisticated experiments is needed to further develop our understanding.

High bias electron transport in qm-SWNTs has been shown to follow a Landauer model, adopted to nanotubes by Yao,¹⁷ Park,¹⁸ Pop and Mann,^{11,13} and others.^{5,7,9,10,19} At high bias voltages (V_b), optical phonon scattering contributes strongly

to the resistance because of the strong electron–phonon coupling originating from the Kohn anomalies in carbon nanotubes,^{5,7,17,18} and results in nonequilibrium phonon populations.^{9–12,14} Recently, surface polar phonons^{20,21} in substrate-supported nanotubes have been identified as a significant electron scattering mechanism, however this is absent in suspended nanotubes. Previous theoretical models and experiments on fully doped qm-SWNTs^{10,11,17,18} ignored the presence of a bandgap, focusing instead on the linear band-structure approximation. However, qm-SWNTs do in fact exhibit small electronic bandgaps.^{22–26} In addition, Deshpande et al. recently showed that Mott insulating behavior in pristine, suspended, qm-SWNTs opens larger bandgaps of ~ 100 meV.²⁷ Since this energy scale is larger than the room temperature thermal energy, the effects of the gap on electron transport are substantial. While many studies have observed the effects of this mini-bandgap on low bias electron transport in qm-SWNTs,^{22–26} a quantitative model for the gate voltage (V_g) dependence of low and high-bias electron transport in qm-SWNTs is still much needed.

In the measurements presented here, an electrical drain current (I_d) is passed through qm-SWNTs by applying a bias voltage, while the nanotubes are doped electrostatically with a backgate. The electrical data is fit to a Landauer model, which incorporates the gate voltage dependence of electron transport in qm-SWNTs. The temperatures of the qm-SWNTs

* To whom correspondence should be addressed. Address: Department of Electrical Engineering, University of Southern California, Los Angeles, CA 90089-0271. Phone: 213-740-8787. E-mail: scronin@usc.edu.

[†] University of Southern California.

[‡] California Institute of Technology.

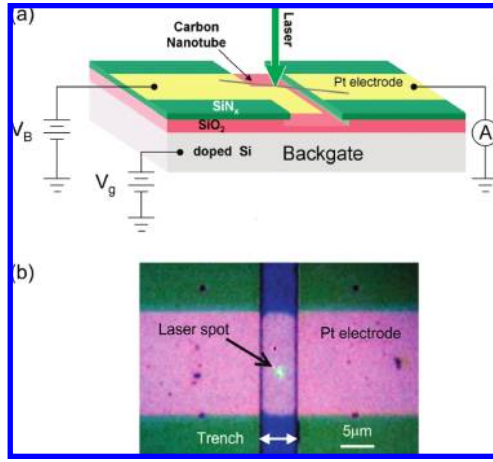


Figure 1. (a) Schematic diagram of the simultaneous optical and electronic carbon nanotube measurements. (b) Optical microscope image of a typical sample measured in this study.

are measured using Raman spectroscopy, enabling us to examine the correlation between the vibrational and electronic properties, and to provide a more detailed understanding of electrical transport behavior.

Samples are fabricated using chemical vapor deposition (CVD) on Pt electrodes with predefined catalyst beds, as reported previously.^{11,14,25,28,29} The resulting devices consist of single-walled nanotubes suspended over trenches 300 nm deep and 2–5 μm wide, as shown in Figure 1a. Raman spectra are collected using a Renishaw *InVia* Raman spectrometer with laser excitation at 532, 633, and 785 nm. All experiments are carried out in an argon environment to avoid burnout of the nanotubes at the high temperatures reached under high applied V_b . Figure 1b shows an optical microscope image of a typical suspended nanotube sample measured in this study. The focused laser spot can be seen positioned in the center of the trench. The nanotube cannot be seen optically but is detected by its strong Raman signal and by scanning electron microscopy.

The G band vibrational modes are known to downshift with increasing temperature due to the anharmonicity of the carbon–carbon bond.^{30,31} Typical values for this rate of downshift lie in the range from -0.022 to -0.044 cm^{-1}/K .^{32–34} These downshifts can, in turn, be used to determine the temperature and phonon populations.^{20,35,36} Figure 2 shows the calibration data of the G band temperature dependence, measured in a temperature controlled stage. For the nanotube shown in Figure 2a, the temperature coefficients of the G_+ and G_- bands are 0.028 and 0.027 cm^{-1}/K , respectively. Using these temperature coefficients, we can later convert the downshifts observed in the G_+ and G_- band frequencies under high voltage bias to temperature.

Figure 3a,b shows the conductance–gate voltage and current–bias voltage data from a nanotube under two different gate voltages, plotted together with the results from the model, outlined below. The conductance shows a strong dip near $V_g = 0$ V, which is caused by the reduced carrier concentration when the Fermi energy (E_F) is in the mini-bandgap. In Figure 3b, the current observed at high bias exhibits negative differential conductance when $V_g = -2$ V

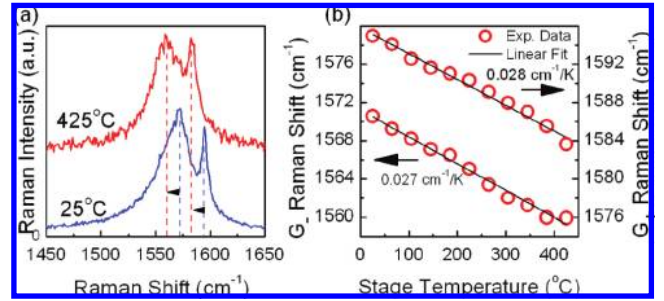


Figure 2. (a) G band Raman spectra showing downshifts with increasing temperature. (b) G band Raman shift versus temperature with linear fits.

(i.e., p-doped) and Ohmic behavior when $V_g = 1/2V_b$ (so that E_F is always in the middle of the gap, i.e., undoped). The significant bandgap in this nanotube causes the conductivity in the doped state to be significantly higher than the intrinsic state. As can be seen in Figure 3a, the model agrees well with the data for low V_b , and qualitatively reproduces the observed Ohmic-to-NDC behavior transition at high V_b .

The data shown in Figure 3 are fit nicely with a numerical Landauer transport model including the effects of a bandgap, as described below. In the Landauer model,^{10–14,17,18,26} the nanotube resistance is expressed as

$$R = R_0^* + R_s + 2R_c \quad (1)$$

where R_s is the resistance arising from scattering in the SWNT, R_c is the contact resistance, and

$$R_0^* = \frac{h}{4q^2} \frac{1}{\int_{\text{bands}} \frac{df}{dE} dE} \quad (2)$$

is the depleted quantum channel resistance. $f(E)$ is the Fermi distribution function, q is the charge of an electron, h is Planck's constant, and the integral is taken over all energies, except those in the bandgap. The scattering contribution to the resistance in a carbon nanotube is given by

$$R_s = R_0^* \left(\frac{1 - T_s^*}{T_s^*} \right) \quad (3)$$

where

$$T_s^* = \int_{\text{bands}} \frac{\lambda_{\text{eff}}}{L + \lambda_{\text{eff}}} \frac{df}{dE} dE \bigg/ \int_{\text{bands}} \frac{df}{dE} dE \quad (4)$$

is the effective scattering coefficient within the depleted quantum channel. This equation can be found using the Landauer model or from the Boltzmann transport equation in one-dimension.³⁷ The electron mean free path λ_{eff} is given by Matthiessen's rule

$$\lambda_{\text{eff}} = (\lambda_{\text{ac}}^{-1} + \lambda_{\text{op,ems}}^{-1} + \lambda_{\text{op,abs}}^{-1})^{-1} \quad (5)$$

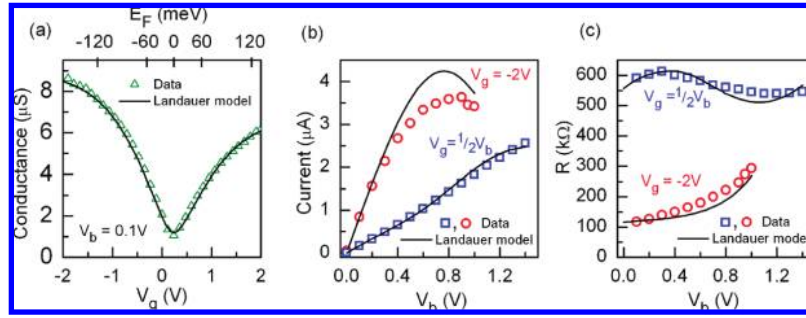


Figure 3. Electrical data and Landauer model results from a suspended quasi-metallic SWNT with (a) conductance plotted versus V_g , (b) I_d plotted versus V_b , and (c) R plotted versus V_b . The doped state (circles) shows NDC, while the intrinsic state (squares) has a linear I_d - V_b relationship.

The acoustic scattering length is given by $\lambda_{ac} = \lambda_{ac}^{RT}(300K/T_{ac})$. The optical phonon scattering length for emitted phonons is given by

$$\lambda_{op,ems} = \frac{E_{ph}L}{qV_t} + \lambda_{op}^{\min} \left(\frac{1 + N_{op}(300K)}{1 + N_{op}(T_{op})} \right) \quad (6)$$

where V_t is the (contact resistance-corrected) voltage drop across the nanotube and $E_{ph} = 0.16$ eV is the optical phonon energy at the zone boundary. For absorbed phonons, it is given by

$$\lambda_{op,abs} = \lambda_{op}^{\min} \left(\frac{1 + N_{op}(300K)}{N_{op}(T_{op})} \right) \quad (7)$$

In these equations, λ_{op}^{\min} is the scattering length for electron scattering from OP emission in the nanotube after the electron has accelerated to the threshold energy, E_{ph} . Low-energy electrons may scatter with this length scale (λ_{op}^{\min}) from the absorption of thermally populated OPs, as described by eq 7. The scattering lengths used in the fit were $\lambda_{ac}^{RT} = 1 \mu\text{m}$ and $\lambda_{op}^{\min} = 35$ nm, in accordance with previous work.^{11,14,18} Other studies examined the energy dependence of the scattering rate.³⁸ However, here we limit ourselves to the constant relaxation time approximation by reducing the scattering length proportionately to the group velocity ($\lambda(E) = \nu(E)\tau$), resulting in short scattering lengths near the band edges.

The quantum contact resistance is given in the Landauer equation^{39,40} by

$$R_c = R_0^* \left(\frac{1 - T_c^*}{T_c^*} \right) \quad (8)$$

where the effective transmission coefficient T_c^* (in the depleted quantum channel) is given by

$$T_c^* = \int_{\text{bands}} \Delta f(V_c) T_c(E) dE / \int_{\text{bands}} \Delta f(V_c) dE \quad (9)$$

where V_c is the contact voltage drop, $\Delta f(V_c) = f(E_F + (1/2)eV_c) - f(E_F - (1/2)eV_c)$, and $T_c(E)$ is the contact transmission

coefficient, which approximates the tunneling through Schottky barriers at the contacts.³⁹⁻⁴² In order to account for the n-type and p-type conductance asymmetry, the two transmission coefficients were fit separately and were generally found to be between 0.1 to 0.2 for our Pt-contacted qm-SWNTs. The voltage drops ($2V_c + V_t = V_b$) and resistances must be solved iteratively. As before (eq 1), to find the total resistance, we sum the individual resistance contributions. In the limit of zero bandgap, $T_c^* \rightarrow T_c$, the V_g dependence of the depleted quantum channel resistance vanishes, with $R_0^* = R_0 = h/(4q^2)$, and the above equations reduce to the familiar Landauer model. We can relate E_F of the nanotube to V_g by numerically solving the equation^{26,43}

$$E_F + \frac{Q(E_F)}{C} = eV_g \quad (10)$$

by integrating over the density of states. Q is the charge induced on the nanotube, C is the geometric gate capacitance, and a hyperbolic band structure is used to model the density of states. The bandgap creates a nonlinear $V_g - E_F$ relationship, which is essential to fitting the data properly. Using these equations and the temperature, measured in situ by Raman spectroscopy, we can model I_d as a function of both V_b and V_g to fit the model to the experimental data taken from a nanotube. These equations can be used to model the transport in semiconducting nanotubes as well; however, larger bandgaps and small n-type transmission coefficients with Pt electrodes prevent accurate bandgap estimation.

The electron and hole transmission coefficients, $T_{c,n}$ and $T_{c,p}$ (respectively), gate capacitance C (26 pF/ μm), and E_{gap} (120 meV) were used as the only fitting parameters, while the temperature was measured using Raman spectroscopy (Figurw 5c,d). The model can be seen to fit the data reasonably well with these parameters, especially at low bias. The transition from Ohmic to NDC behavior can be explained qualitatively by considering the temperature dependence of the resistance. The resistance of metals typically increases linearly with T because of increased phonon scattering, while that of intrinsic semiconductors decreases exponentially with T , because of thermally promoted carrier density increase. For qm-SWNTs with E_F in the middle of the mini-bandgap (i.e., intrinsic), the two effects compete, giving rise to a nearly constant resistance profile

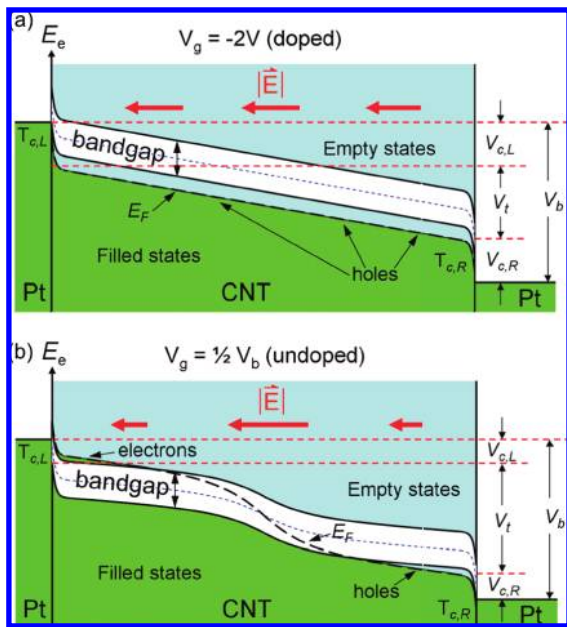


Figure 4. Schematic of electronic potential versus position along the nanotube length for the (a) doped ($V_g = -2\text{ V}$) and (b) undoped ($V_g = 1/2 V_b$) cases. The electric field strength is indicated by the bold arrows in the top of each figure.

despite heating (Figure 3c). For qm-SWNTs with E_F in the band (doped), the system acts like a metal, exhibiting an increase in resistance due to self-heating. These effects are captured by the above model and are illustrated in the model curves of Figure 3c. Two additional data sets from quasi-metallic nanotubes exhibiting this effect are shown in the Supporting Information section. All nanotubes examined in this study exhibited suppression of NDC while undoped.

Equation 4 makes the simplifying assumption that E_F is constant with respect to the bandgap throughout the length of the SWNT. However, the voltage drop along the SWNT effectively changes the gate voltage, causing the Fermi energy to change also, as outlined by Tersoff et al.⁴⁴ This is accounted for with a finite element analysis (FEA), which includes this spatial dependence of E_F , as calculated using eq 10. In the FEA model at low bias, E_F is found to change by only a few millielectron volts (with respect to the band edge) along the length of the SWNT and is well approximated as constant. However, at high biases E_F varies by as much as 100 meV (at $V_b = 1.4\text{ V}$) along the length of the SWNT.

Figure 4 illustrates several effects of high bias transport in the nanotube. First of all, in the electrostatically doped nanotube (Figure 4a), small changes in Fermi energy induce relatively large charging voltages (because the capacitance in eq 10 is small). Thus, the Fermi energy remains nearly constant along the length of the nanotube. In an undoped nanotube (Figure 4b), however, the Fermi energy is in the bandgap. Therefore, changes in the Fermi energy do not induce much charge on the nanotube. As a result, the Fermi energy varies strongly with the voltage drop across the nanotube. Second, Figure 4 indicates the magnitude and direction of the electric field in the nanotube. In the doped nanotube (Figure 4a), the resistance and electric field are

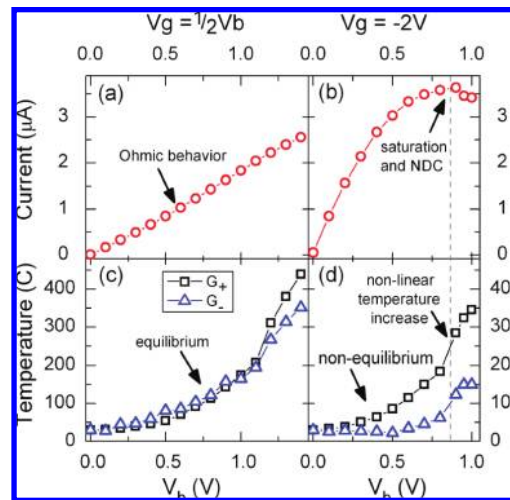


Figure 5. Electrical current (a,b) and Raman downshift calculated temperature (c,d) for the same SWNT at two different values of V_g . The undoped nanotube shows equal phonon heating and an Ohmic I_d-V_b , while the gated (doped) nanotube exhibits nonequilibrium heating and negative differential conductance.

fairly constant along the length of the nanotube. In the undoped nanotube, however, the resistance increases when the Fermi energy crosses the bandgap, due to charge carrier depletion. Because of this increased resistance, the electric field becomes stronger in this location, and a larger fraction of the bias voltage drop occurs in the nanotube instead of at the contacts.

The Raman data also display interesting behavior with respect to doping conditions. Figure 5a,b shows the I_d-V_b characteristics taken from the same nanotube under undoped (intrinsic, $V_g = 1/2 V_b$, Figure 5a) and doped ($V_g = -2\text{ V}$, Figure 5b) gating conditions. At high V_b , the G_+ and G_- bands are observed to downshift due to Joule heating in the nanotube. The effective temperature of the SWNT measured from these two bands is determined from their downshifts and the temperature coefficients established in Figure 2b, and are plotted in Figure 5c,d for the undoped and doped gating conditions, respectively. In Figure 4c, the temperatures of the G_+ and G_- bands increase together in thermal equilibrium up to about 400 °C. Whereas, at $V_g = -2\text{ V}$ (Figure 5d), the two phonon modes give different temperatures over the whole voltage range with a sharp increase in the temperature occurring with the onset of NDC. So, in addition to changing the I_d-V_b characteristics, the gate voltage can be used to switch between thermal equilibrium and nonequilibrium phonon populations.

As pointed out by the large body of literature on this subject,⁹⁻¹⁴ the cause of the observed negative differential conductance in suspended SWNTs is self-heating via a threshold optical phonon emission process (eq 6), which causes hot, nonequilibrium phonon populations. Here, we observe the switch from Ohmic/equilibrium behavior to NDC/nonequilibrium behavior, supporting this theory. While current saturation occurs in any suspended metallic filament system, even ordinary tungsten light bulbs, the criterion for the occurrence of NDC is an additional, nonlinear increase in resistance. In this case, threshold optical phonon emission

and the resulting nonequilibrium phonon populations serve this purpose.

In conclusion, we have shown that the gate voltage conditions drastically influence the high bias voltage characteristics of carbon nanotubes, and that the phonon distribution can also change substantially. Ohmic behavior is observed in undoped qm-SNWTs, while negative differential conductance (NDC) is observed in qm-SWNTs doped with a gate voltage. To explain this behavior, we present a model for the electric current in a nanotube as a function of both applied V_b and V_g and compare the results to experimental data taken from a qm-SWNT. The sudden increase in the phonon population of the nanotube corresponds with the onset of NDC, supporting the theory that NDC is caused by nonequilibrium phonon populations and selective electron–phonon coupling in the nanotube.

Acknowledgment. This research was supported in part by DOE Award No. DE-FG02–07ER46376 and the National Science Foundation Graduate Research Fellowship Program. A portion of this work was done in the UCSB nanofabrication facility, part of the NSF funded NNIN network.

Supporting Information Available: Electrical data from two additional suspended, metallic single-walled carbon nanotubes. This material is available free of charge via the Internet at <http://pubs.acs.org>.

References

- (1) Piscanec, S. *Phys. Rev. Lett.* **2004**, *93* (18), 185503.
- (2) Caudal, N. *Phys. Rev. B* **2007**, *75* (11), 115423–11.
- (3) Samsonidze, G. G. *Phys. Rev. B* **2007**, *75* (15), 155420–8.
- (4) Bushmaker, A. W. *Nano Lett.* **2009**, *9* (2), 607–611.
- (5) Dubay, O. *Phys. Rev. Lett.* **2002**, *88* (23), 235506.
- (6) Barnett, R. *Phys. Rev. B* **2005**, *71* (3), 22.

- (7) Piscanec, S. *Phys. Rev. B* **2007**, *75* (3), 035427.
- (8) Javey, A. *Phys. Rev. Lett.* **2004**, *92* (10), 106804–4.
- (9) Lazzeri, M.; Mauri, F. *Phys. Rev. B* **2006**, *73* (16), 165419.
- (10) Lazzeri, M. *Phys. Rev. Lett.* **2005**, *95*, 236802.
- (11) Pop, E. *Phys. Rev. Lett.* **2005**, *95* (15), 155505.
- (12) Oron-Carl, M.; Krupke, R. *Phys. Rev. Lett.* **2008**, *100* (12), 127401–4.
- (13) Mann, D. J. *Phys. Chem. B* **2006**, *110* (4), 1502–1505.
- (14) Bushmaker, A. W. *Nano Lett.* **2007**, *7* (12), 3618–3622.
- (15) Zhong, Z. H. *Nat. Nanotechnol.* **2008**, *3* (4), 201–205.
- (16) Rosenblatt, S. *Appl. Phys. Lett.* **2005**, *87* (15), 153111.
- (17) Yao, Z. *Phys. Rev. Lett.* **2000**, *84* (13), 2941.
- (18) Park, J. Y. *Nano Lett.* **2003**, *4* (3), 517.
- (19) Reich, S. et al. *Carbon Nanotubes: Basic Concepts and Physical Properties*; Wiley-VCH: New York, 2004.
- (20) Steiner, M., et al. *Nat. Nano* **2009**, *4* (5), 320–324.
- (21) Perebeinos, V. *Nano Lett.* **2009**, *9* (1), 312–316.
- (22) Blase, X. *Phys. Rev. Lett.* **1994**, *72* (12), 1878.
- (23) Ouyang, M. *Science* **2001**, *292* (5517), 702–705.
- (24) Zhou, C. *Phys. Rev. Lett.* **2000**, *84* (24), 5604.
- (25) Cao, J. *Small* **2005**, *1* (1), 138–141.
- (26) Biercuk, M. J. *Top. Appl. Phys.* **2008**, *111*, 455.
- (27) Deshpande, V. V. *Science* **2009**, *323* (5910), 106–110.
- (28) Kong, J. *Nature* **1998**, *395* (6705), 878–881.
- (29) Qi, P. *Nano Lett.* **2003**, *3* (3), 347–351.
- (30) Bonini, N. *Phys. Status Solidi B* **2008**, *245* (10), 2149–2154.
- (31) Bonini, N. *Phys. Rev. Lett.* **2007**, *99* (17), 176802–4.
- (32) Hsu, I.-K. *Appl. Phys. Lett.* **2008**, *92*, 063119.
- (33) Atashbar, M. Z.; Singamaneni, S. *Appl. Phys. Lett.* **2005**, *86* (12), 123112–3.
- (34) Chiashi, S. *Chem. Phys. Lett.* **2004**, *386* (1–3), 89–94.
- (35) Deshpande, V. V. *Phys. Rev. Lett.* **2009**, *102* (10), 105501–4.
- (36) Pomeroy, J. W. *Phys. Status Solidi B* **2008**, *245* (5), 910–912.
- (37) Seri, T.; Ando, T. *J. Phys. Soc. Jpn.* **1997**, *66* (1), 169–173.
- (38) Perebeinos, V. *Phys. Rev. Lett.* **2005**, *94* (8), 086802.
- (39) Bachtold, A. *Phys. Rev. Lett.* **2000**, *84* (26), 6082.
- (40) Buldum, A.; Lu, J. P. *Phys. Rev. B* **2001**, *63* (16), 161403.
- (41) Martel, R. *Phys. Rev. Lett.* **2001**, *87* (25), 256805.
- (42) Derycke, V. *Appl. Phys. Lett.* **2002**, *80* (15), 2773–2775.
- (43) Das, A. *Nat. Nano* **2008**, *3* (4), 210–215.
- (44) Tersoff, J. *Appl. Phys. Lett.* **2005**, *86* (26), 263108–3.

NL901042W